

# ATP steal between cation pumps: a mechanism linking $\text{Na}^+$ influx to the onset of necrotic $\text{Ca}^{2+}$ overload

J Castro<sup>1</sup>, I Ruminot<sup>1</sup>, OH Porras<sup>1</sup>, CM Flores<sup>1</sup>, T Hermosilla<sup>1</sup>, E Verdugo<sup>1</sup>, F Venegas<sup>2</sup>, S Härtel<sup>1</sup>, L Michea<sup>2</sup> and LF Barros<sup>\*1</sup>

<sup>1</sup> Centro de Estudios Científicos CECS, Casilla 1469, Valdivia, Chile

<sup>2</sup> Laboratory of Molecular and Integrative Physiology, Faculty of Medicine, University of Los Andes, Santiago, Chile

\* Corresponding author: LF Barros, Centro de Estudios Científicos CECS, Casilla 1469, Valdivia, Chile. Tel: 56 63 234500; Fax: 56 63 234517; E-mail: fbarros@cecs.cl

Received 18.8.05; revised 14.10.05; accepted 30.11.05

Edited by JA Cidlowski

## Abstract

We set out to identify molecular mechanisms underlying the onset of necrotic  $\text{Ca}^{2+}$  overload, triggered in two epithelial cell lines by oxidative stress or metabolic depletion. As reported earlier, the overload was inhibited by extracellular  $\text{Ca}^{2+}$  chelation and the cation channel blocker gadolinium. However, the surface permeability to  $\text{Ca}^{2+}$  was reduced by 60%, thus discarding a role for  $\text{Ca}^{2+}$  channel/carrier activation. Instead, we registered a collapse of the plasma membrane  $\text{Ca}^{2+}$  ATPase (PMCA). Remarkably, inhibition of the  $\text{Na}^+/\text{K}^+$  ATPase rescued the PMCA and reverted the  $\text{Ca}^{2+}$  rise. Thermodynamic considerations suggest that the  $\text{Ca}^{2+}$  overload develops when the  $\text{Na}^+/\text{K}^+$  ATPase, by virtue of the  $\text{Na}^+$  overload, clamps the ATP phosphorylation potential below the minimum required by the PMCA. In addition to providing the mechanism for the onset of  $\text{Ca}^{2+}$  overload, the crosstalk between cation pumps offers a novel explanation for the role of  $\text{Na}^+$  in cell death.

*Cell Death and Differentiation* advance online publication, 20 January 2006; doi:10.1038/sj.cdd.4401852

**Keywords:** necrosis; oxidative stress; metabolic stress; HeLa cells; MDCK cells;  $\text{Na}^+/\text{K}^+$  ATPase; PMCA

**Abbreviations:** KRH, Krebs–Ringer–Hepes buffer; NCX,  $\text{Na}^+/\text{Ca}^{2+}$  exchanger; PMCA, plasma membrane  $\text{Ca}^{2+}$  ATPase; VOCC, voltage-operated  $\text{Ca}^{2+}$  channel; NVI, necrotic volume increase; LDH, lactate dehydrogenase; PI, propidium iodide

## Introduction

Necrosis, sometimes termed oncosis, is the mode of cell death that prevails under severe pathological conditions such as ischemia, anoxia, trauma and acute microbial infection.<sup>1</sup> In addition to its pathogenic role, necrosis is instrumental for the efficient activation of the immune response against microorganisms and tumour cells, so it may be considered 'physiological' in the broadest sense of the term. Character-

ized by metabolic collapse, swelling of cytosol and organelles, membrane blebbing, activation of proteolytic enzymes and ultimately by cell lysis, it is becoming accepted that necrosis is not a chaotic process but a predetermined cascade of well-defined biochemical events.<sup>2–4</sup>

$\text{Ca}^{2+}$  overload is a key feature of cell necrosis, a fact underscored by the strong protection afforded by withdrawal of extracellular  $\text{Ca}^{2+}$ , chelation of intracellular  $\text{Ca}^{2+}$  or inhibition of  $\text{Ca}^{2+}$  channels and transporters.<sup>5,6</sup> The  $\text{Ca}^{2+}$  rise that precedes necrosis is typically biphasic. In the first 5 min, the concentration of  $\text{Ca}^{2+}$  in the cytosol doubles to a new steady state at about 200 nM, a metastable phase that lasts for 10–30 min. In HeLa cells, MDCK cells and human erythrocytes exposed to high concentrations of hydrogen peroxide, the early phase involves GSH-sensitive release of  $\text{Ca}^{2+}$  from cytosolic sites.<sup>7</sup> In the second phase, cytosolic  $\text{Ca}^{2+}$  rises steadily to reach mM levels before disruption of the cell membrane. Various terms regenerative  $\text{Ca}^{2+}$  rise, unregulated  $\text{Ca}^{2+}$  increase or delayed  $\text{Ca}^{2+}$  overload, the secondary phase requires the presence of extracellular  $\text{Ca}^{2+}$ , which is thought to enter the cytosol through channels and transporters. Cell surface examples are the  $\text{Na}^+/\text{Ca}^{2+}$  exchanger (NCX) cycling in its reversed mode, voltage-operated  $\text{Ca}^{2+}$  channels (VOCC) and several  $\text{Ca}^{2+}$ -permeable cation channels of recent description.<sup>5,8–10</sup> Regardless of the entry pathway, sustained high levels of cytosolic  $\text{Ca}^{2+}$  are toxic, leading to mitochondrial disruption, further activation of ion channels and activation of degradative enzymes including proteases, lipases, ATPases and DNAses.<sup>6</sup>

However complex the  $\text{Ca}^{2+}$  overload becomes as it evolves with time, the number of mechanisms at work is likely to be minimum at its onset, that is, when  $\text{Ca}^{2+}$  levels are still within physiological range. With this in mind, we set out to identify biochemical mechanisms associated with the onset of the delayed  $\text{Ca}^{2+}$  overload in epithelial cells. Several groups, including our own, had reported the early activation of ion channels that pass  $\text{Na}^+$ ,  $\text{K}^+$  and  $\text{Cl}^-$  during necrosis and thus we hoped to discover a role for  $\text{Ca}^{2+}$ -permeable cation channels, such as those evidenced in pancreatic cells and neurons under stress.<sup>8,9</sup> However, the experiments showed that during the early overload,  $\text{Ca}^{2+}$  permeability was reduced and that the  $\text{Ca}^{2+}$  overload was explained by a collapse in  $\text{Ca}^{2+}$  extrusion by the plasma membrane  $\text{Ca}^{2+}$  ATPase (PMCA). Most interestingly, the PMCA collapse was only functional and required the activity of the  $\text{Na}^+/\text{K}^+$  pump, a reversible mechanism that contrasts with the permanent inactivation of the PMCA by caspases and calpain observed in later stages of apoptosis and necrosis.<sup>11</sup> This inhibitory crosstalk between the two cation pumps provides a novel mechanistic explanation for the long known pro-necrotic effect of  $\text{Na}^+$ . Part of this work was presented in an abstract form (*Mechanism of Cell Death: Molecular Insights and Therapeutic Perspectives*, Reñaca, Chile, April 2005).

## Results

The study was based on HeLa cells, a well-known epithelial cell line in terms of Ca<sup>2+</sup> homeostasis and cell death. Some experiments were reproduced in MDCK, a more differentiated epithelial cell line. Ca<sup>2+</sup> overload was triggered by oxidative stress and metabolic stress, and both stimuli induced similar mechanisms. Previously, we reported that the induction of necrotic changes in time frames similar to those observed in acute human pathologies, including early Ca<sup>2+</sup> rise (<1 min), ATP depletion (about 1 min), mitochondrial depolarization (20–30 min), necrotic bleb formation (60 min) and cell lysis (2–3 h), requires over 10 mM hydrogen peroxide.<sup>7,12</sup> In HeLa cells and several other cell lines, this relative resistance to hydrogen peroxide results from their enrichment in glutathione.<sup>7</sup> To allow direct comparison with two previous studies of HeLa and MDCK cells,<sup>7,12</sup> the concentration of hydrogen peroxide chosen to induce necrosis was 32 mM throughout the study. Control experiments were described in previous reports<sup>12</sup> and also in Materials and Methods, which discard possible interference between peroxide and the fluorescent dyes.

In response to oxidative stress, HeLa cells reacted with a biphasic increase in cytosolic Ca<sup>2+</sup> (Figure 1a). Reportedly, the first phase of the rise is caused by GSH-sensitive release of Ca<sup>2+</sup> from cytosolic moieties.<sup>7</sup> Here, we focused on the second phase, the delayed or regenerative phase of Ca<sup>2+</sup> increase. Monitored in a large number of cells, the onset of the delayed Ca<sup>2+</sup> overload occurred 20–40 min after injury onset

(Figure 1b). Withdrawal of the oxidant during the delayed Ca<sup>2+</sup> overload (at 30 min) did not change the rate of Ca<sup>2+</sup> accumulation, nor precluded onset of the overload in the less responsive cells (Figure 1c). Hence, the delayed Ca<sup>2+</sup> overload does not require the continuous presence of the oxidant. This observation was of operational importance because it allowed some experiments to be carried out in the absence of peroxide (see below). In the presence of ethyleneglycol-bis(b-aminoethyl ether)-*N,N,N',N'*-tetraacetic acid (EGTA), the second phase of the Ca<sup>2+</sup> rise did not occur (Figure 1d), pointing to an extracellular source. Reduction of extracellular Ca<sup>2+</sup> from 1.25 mM to 50 μM inhibited peroxide-induced necrosis by 71 ± 15 [*n* = 3]%. Once started, the increase in cytosolic Ca<sup>2+</sup> was reverted both by a low-Ca<sup>2+</sup> medium or by the broad-specificity non-permeant cation channel blocker gadolinium (Figure 1e and f). These experiments confirmed that the delayed Ca<sup>2+</sup> rise induced by oxidative stress requires extracellular Ca<sup>2+</sup> and indicated a possible role for gadolinium-sensitive Ca<sup>2+</sup> channels. Plasma membrane permeabilization, the final event in necrotic cell death, began 2 h after continuous exposure to H<sub>2</sub>O<sub>2</sub> (Figure 2a and b). However, a protocol of transient exposures showed that 20–40 min were sufficient to commit the cells to necrosis (Figure 2c). Thus, commitment roughly coincided with the onset of delayed Ca<sup>2+</sup> overload (Figure 1b).

Cell swelling, also termed necrotic volume increase (NVI), is one morphological feature that differentiates necrosis from apoptosis.<sup>4,13</sup> In the later stages of the necrotic process, large

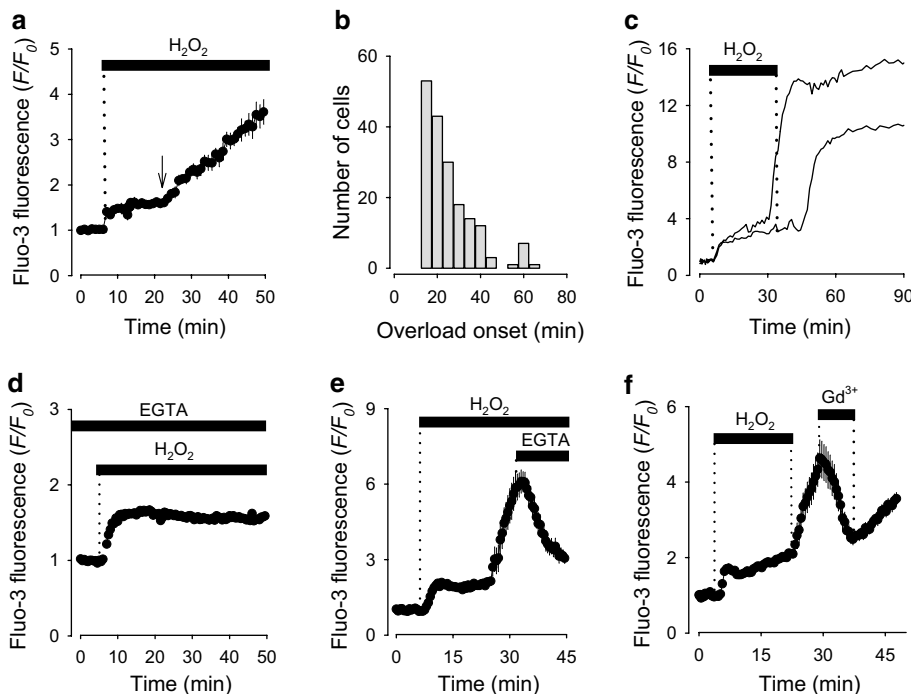


**Figure 1** The delayed Ca<sup>2+</sup> overload in HeLa cells requires Ca<sup>2+</sup> influx. Cytosolic Ca<sup>2+</sup> fluorescence was monitored as described in Materials and Methods. (a) In response to hydrogen peroxide, a biphasic increase in cytosolic Ca<sup>2+</sup> is observed. In this experiment, the onset of the delayed Ca<sup>2+</sup> overload was recorded 17 min after injury onset (arrow). (b) Times of onset of delayed Ca<sup>2+</sup> overload onset in 184 cells in 17 experiments. (c) Withdrawal of the oxidant after 30 min of exposure did not change the rate of Ca<sup>2+</sup> rise nor precluded its onset. Lines represent two individual cells, from three experiments with 8–10 cells each. (d) Chelation of extracellular Ca<sup>2+</sup> with 10 mM EGTA precluded the onset of delayed Ca<sup>2+</sup> overload. Similar data were obtained in two other experiments. The delayed Ca<sup>2+</sup> overload was reverted with 10 mM EGTA (e) or 10 μM Gd<sup>3+</sup> (f). Data are representative of five and three experiments, respectively

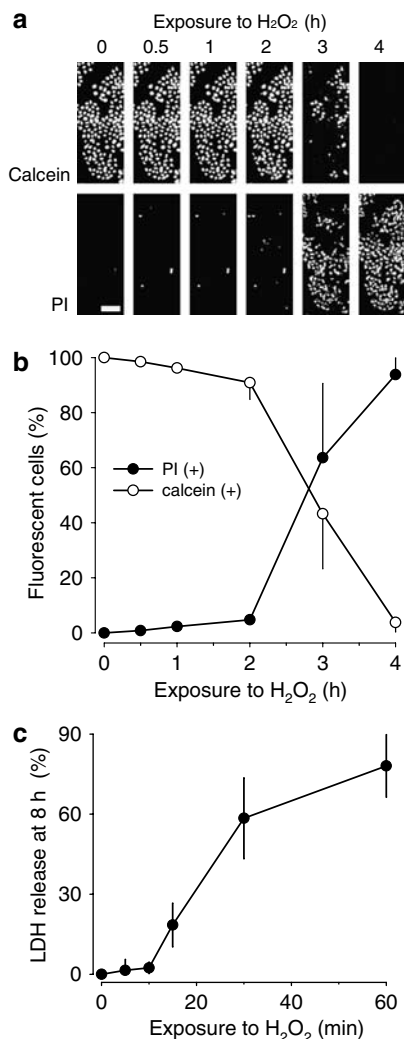


**Figure 2** The onset of delayed Ca<sup>2+</sup> overload coincides with necrotic commitment. (a) Calcein-loaded cells were exposed to H<sub>2</sub>O<sub>2</sub> in the presence of 10 μg/ml propidium iodide (PI). Confocal images were acquired at the times given. Bar is 100 μm. (b) Summary of three experiments similar to the one illustrated in (a). (c) Cells were exposed to H<sub>2</sub>O<sub>2</sub> for 0, 5, 10, 15, 30 or 60 min and then washed thrice with KRH buffer. After completing 8 h, the activity of lactate dehydrogenase (LDH) was measured in the supernatant and expressed relative to that released with digitonin. Data are from two experiments performed in duplicate

blebs grow monotonically until the plasma membrane is disrupted,<sup>12</sup> but it is not clear when NVI starts and how it relates to the Ca<sup>2+</sup> rise. This is particularly true for adherent cells in which cell volume cannot be inferred from cell diameter. To address the issue, we first tried to measure relative volume by confocal microscopy in calcein-loaded HeLa cells, but found that oxidative stress led to rapid dye loss, precluding accurate measurements over extended periods (data not shown). For this reason, a method was developed to measure absolute volume based on three-dimensional confocal reconstructions of HeLa cells stained with a lipophilic dye. The data presented in Figure 3 show that NVI begins earlier than the delayed Ca<sup>2+</sup> overload. Because Na<sup>+</sup> is the main effective osmolyte of the extracellular milieu, this result suggested a Na<sup>+</sup> gain before the Ca<sup>2+</sup> gain. By

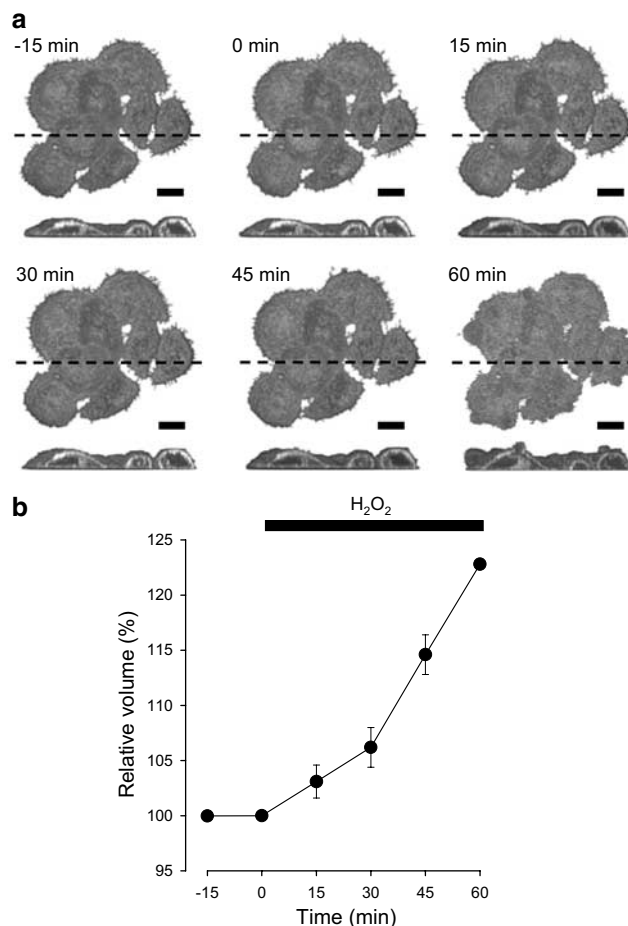


**Figure 3** Cell swelling starts before the delayed Ca<sup>2+</sup> overload in HeLa cells. Absolute volume was measured by reconstructing three-dimensional confocal microscopy stacks of DiIC<sub>18</sub>-stained HeLa cells as described in Materials and Methods. (a) A cluster of cells was imaged before and during exposure to H<sub>2</sub>O<sub>2</sub>, which started at 0 min. For each time, the xy-projection is shown together with a cross-section in the xz-plane taken at the indicated y-position (dashed line). Bars represent 20 μm. (b) Normalized volumes for four (0, 15, 30 and 45 min) and two experiments (-15 and 60 min). In each experiment, 4–13 cells were measured. For 24 control cells, the volume measured was 4.0 ± 1.0 pl

60 min, cells have swollen by 25% and blebs become apparent (Figure 3), which is in register with previous measurements using phase contrast microscopy.<sup>12</sup> The absence of an early shrinkage indicates that the Na<sup>+</sup> gain outweighs the severe K<sup>+</sup> loss that characterizes oxidative stress.<sup>14</sup> To our knowledge, this is the first report of real-time volume measurements during oxidative stress in adherent cells. Consistent with the early swelling, significant increases in cell Na<sup>+</sup> (Figure 4a) and Na<sup>+</sup> permeability (Figure 4b) were detected early during oxidative stress. Of note, Na<sup>+</sup> replacement by K<sup>+</sup> precluded the delayed Ca<sup>2+</sup> rise (Figure 4c), whereas Na<sup>+</sup> withdrawal during the Ca<sup>2+</sup> rise effectively reverted the rise (Figure 4d). HeLa cell necrosis was significantly inhibited (%) by equimolar replacement of extracellular Na<sup>+</sup> with K<sup>+</sup> (71 ± 16 [n = 3]) or Cs<sup>+</sup> (59 ± 13 [n = 3]), confirming a pathogenic role for Na<sup>+</sup>.

After noting that the Ca<sup>2+</sup> overload required extracellular Ca<sup>2+</sup> and that it was inhibited by the Ca<sup>2+</sup> channel blocker

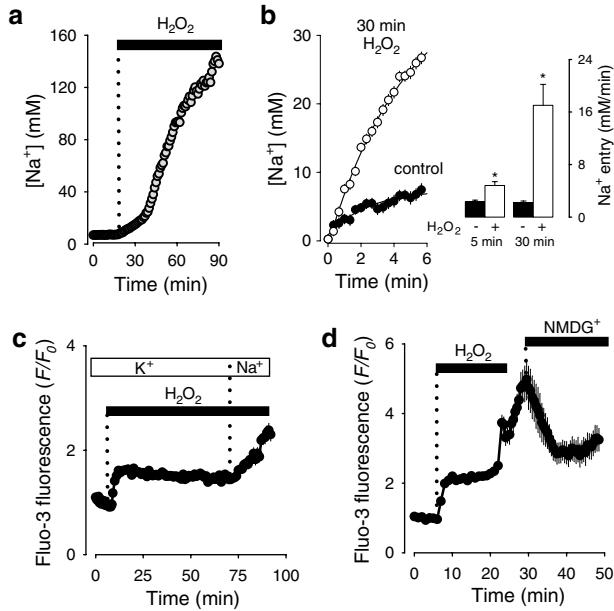


**Figure 4** Na<sup>+</sup> overload is required for delayed Ca<sup>2+</sup> overload in HeLa cells. (a) Cytosolic Na<sup>+</sup> was measured with SBF1 as described in Materials and Methods. Data are representative of six similar experiments. (b) After 30 min exposure to peroxide or vehicle in Na<sup>+</sup>-free KRH (replaced by NMDG<sup>+</sup>), cells were brought back to KRH and cytosolic Na<sup>+</sup> was monitored in the presence of 1 mM ouabain. Data are from 24 cells; the lines correspond to the best fits of two-parameter exponentials. Initial rates of Na<sup>+</sup> entry after 5 and 30 min of peroxide are given in the bar graph (four experiments, with over 15 cells each; \**P* < 0.05 with respect to control). Similar results were obtained with K<sup>+</sup> instead of NMDG<sup>+</sup> (not shown). (c) Cells were exposed to peroxide in Na<sup>+</sup>-free KRH (replaced with K<sup>+</sup>). Note that in the absence of Na<sup>+</sup>, only the first phase of Ca<sup>2+</sup> increase is observed. After 60 min of injury, the exchange of K<sup>+</sup> by Na<sup>+</sup> triggered the delayed Ca<sup>2+</sup> overload. Data are representative of three similar experiments. (d) The delayed Ca<sup>2+</sup> overload was also reverted by equimolar Na<sup>+</sup> substitution by NMDG<sup>+</sup>. Data are representative of three experiments

gadolinium, we expected to detect the activation of Ca<sup>2+</sup> channels.<sup>8–10</sup> However, the Ca<sup>2+</sup> permeability measured with a radioactive tracer was lower than control (Figure 5a), a result that was confirmed independently by a decrease in the rate of Mn<sup>2+</sup> uptake (Figure 5b), a divalent that permeates through Ca<sup>2+</sup> channels. The permeability to divalents was not affected by peroxide removal (Figure 5c), consistent with the lack of effect of such a manoeuvre on the observed rate of Ca<sup>2+</sup> accumulation (see Figure 1c). With enhanced Ca<sup>2+</sup> influx no longer a feasible explanation for the overload, experiments were carried out to check Ca<sup>2+</sup> extrusion. First, the clearance capacity of the cell was evaluated in response to the sudden increase in cytosolic Ca<sup>2+</sup> that follows mechanical stimulation. Figure 6a shows that in HeLa cells, mechanical stimulation induced a rapid and reproducible increase in cytosolic Ca<sup>2+</sup> to about four times the basal value. Assuming a *K*<sub>D</sub> of 1 μM and a basal Ca<sup>2+</sup> concentration of 100 nM,<sup>12</sup> it can be calculated that the peak reached approximately 600 nM. In control cells, this load was typically cleared within 2 min (Figure 6a). In the presence of peroxide, clearance became slower over time (Figure 6b and c). In agreement with the accepted notion that mitochondria do not play a significant role at low Ca<sup>2+</sup> concentrations, uncoupling of the mitochondria with FCCP did not significantly affect the rate of clearance

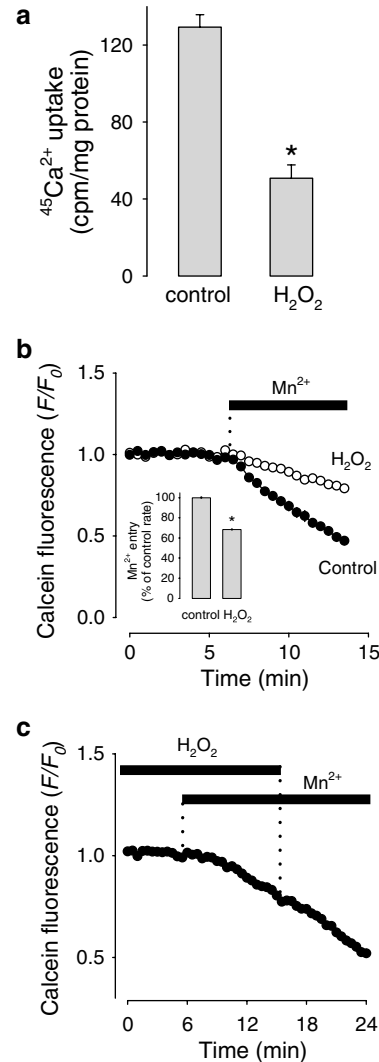


**Figure 5** The permeability of HeLa cells to Ca<sup>2+</sup> and Mn<sup>2+</sup> decreases during oxidative stress. (a) The uptake of <sup>45</sup>Ca<sup>2+</sup> was measured as described in Materials and Methods. Data are from three experiments performed in duplicate. \**P* < 0.05 with respect to control. (b) Calcein fluorescence was measured by confocal microscopy. On addition of 5 mM MnCl<sub>2</sub>, calcein was quenched faster in control cells (closed symbols) than in cells pretreated with peroxide for 30 min (open symbols). The inset shows the average of 48 cells from four experiments for each condition. \**P* < 0.05 with respect to control. (c) The rate of Mn<sup>2+</sup> entry did not change after withdrawal of the oxidant. Data are representative of three experiments

(Figure 6d). Because the Ca<sup>2+</sup> pump at the endoplasmic reticulum also requires higher Ca<sup>2+</sup> levels for activation, these experiments suggested that the PMCA was the likely target of oxidative stress. To demonstrate this point, PMCA activity was measured using fluorescence microscopy.<sup>15</sup> In Figure 7a, the protocol was repeated several times, demonstrating reproducibility of the measurement over a long period. Then, it quantitatively demonstrated that stressed cells lose most of their PMCA activity over the first 30 min of injury (Figure 7b and c).

Knowing that Na<sup>+</sup> overload was required for Ca<sup>2+</sup> overload and that the latter was due to PMCA failure, attention became focused on the mechanistic link between Na<sup>+</sup> and

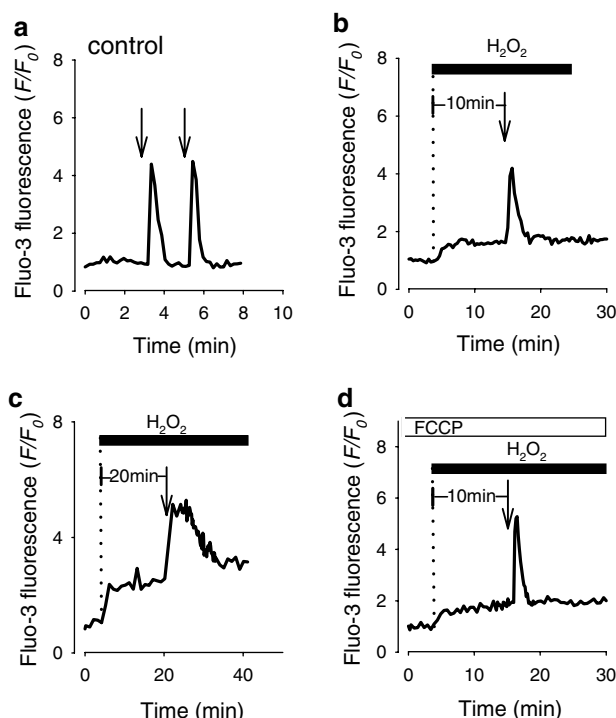


**Figure 6** Delayed failure of Ca<sup>2+</sup> clearance during oxidative stress in HeLa cells. Cytosolic Ca<sup>2+</sup> fluorescence was estimated with Fluo-3 as described in Materials and Methods. (a) A single cell was stimulated twice with a glass micropipette (arrows), demonstrating that after a transient increase, cytosolic Ca<sup>2+</sup> returns to control values. (b) After 10 min exposure to peroxide, the cell was still capable of regulating Ca<sup>2+</sup> after the perturbation. (c) After 20 min, the capacity of Ca<sup>2+</sup> clearance was clearly diminished. Mechanical stimulation after 20 min invariably resulted in rapid Ca<sup>2+</sup> overloading and cell lysis (not shown). (d) An experiment similar to that in (b) but in a cell pretreated with 2 μM of the mitochondrial uncoupler FCCP shows that mitochondria do not play a major role in the clearance of this type of Ca<sup>2+</sup> pulse. Analogous results were obtained in more than eight cells for each protocol

the PMCA. Other than promoting cell depolarization and Ca<sup>2+</sup> entry, Na<sup>+</sup> can be toxic at several levels, for example by inducing mitochondrial depolarization, activating second messengers or even inducing the K<sup>+</sup> loss that mediates apoptosis.<sup>16</sup> The experiments illustrated in Figure 8 show that in HeLa cells exposed to oxidative stress, the inhibition of the PMCA and the ensuing Ca<sup>2+</sup> overload are due to the activity of the Na<sup>+</sup>/K<sup>+</sup> pump. Figure 8a shows that inhibition of the Na<sup>+</sup>/K<sup>+</sup> pump with ouabain caused a 30-fold increase in PMCA activity, reaching 60% of the rate observed in healthy cells (inset). This result is remarkable because in HeLa cells exposed to this concentration of peroxide, bulk ATP levels plummet with a half-time of 2 min, becoming undetectable at 15 and 30 min.<sup>12</sup> As expected from the rescue of PMCA activity, inhibition of the Na<sup>+</sup> pump effectively reverted the Ca<sup>2+</sup> rise (Figure 8b and c). Rubidium uptake experiments showed that oxidative stress induced only a moderate decrease in the activity of the Na<sup>+</sup>/K<sup>+</sup> pump, which stabilized at 50% of control value after 15 min (Table 1). Therefore, oxidative cell injury did not cause permanent damage of the PMCA and the activity of the Na<sup>+</sup>/K<sup>+</sup> pump somehow interfered with the PMCA. Consistently, ouabain inhibited HeLa cell necrosis by 41 ± 5 [3]%. In summary, the activity of

the Na<sup>+</sup>/K<sup>+</sup> pump causes PMCA inhibition, which results in regenerative Ca<sup>2+</sup> overload and cell death.

To investigate whether a similar mechanism was at work in other models of necrotic cell death, experiments were carried out in HeLa cells exposed to metabolic stress, brought about by simultaneous inhibition of glycolysis and mitochondrial respiration. Figure 9 shows that metabolic depletion caused a biphasic Ca<sup>2+</sup> rise similar in amplitude and time course to that elicited by oxidative stress. As with oxidative stress, the secondary Ca<sup>2+</sup> overload required extracellular Ca<sup>2+</sup> and was preceded by Na<sup>+</sup> overload (Figure 9a and b). Again, the Ca<sup>2+</sup> overload evolved with reduced surface permeability to divalents (Figure 9c), was fuelled by Na<sup>+</sup> but not by K<sup>+</sup> (Figure 9d), and was inhibited by ouabain or potassium withdrawal (Figure 9e and f). Therefore, it seems apparent that the delayed Ca<sup>2+</sup> overload in response to metabolic stress obeys mechanisms similar to those induced by oxidative stress. Furthermore, the delayed Ca<sup>2+</sup> overload elicited by oxidative stress in MDCK, a kidney cell line, behaved in a similar manner (Figure 10), suggesting that the underlying mechanism is not constrained to a single cell line.

An economical explanation for the inhibitory effects of Na<sup>+</sup> removal and Na<sup>+</sup>/K<sup>+</sup> pump inhibition is that the onset of Ca<sup>2+</sup> overload is triggered by the activity of the Na<sup>+</sup> pump. But one problem with this hypothesis is that at about 100 μM, the ATP affinity constants of both pumps are similar, meaning that as the concentration of ATP approaches the low micromolar level, both pumps should be inhibited to the same extent. So, how can the cells keep pumping Na<sup>+</sup> (and using ATP) while failing to pump Ca<sup>2+</sup>? In the absence of a kinetic explanation, we analysed the thermodynamics of ion pumping. The time course of the free energy required for Na<sup>+</sup>/K<sup>+</sup> pump cycling was calculated from the intracellular concentrations of Na<sup>+</sup> and K<sup>+</sup>, estimated with SBF1. In the same cells, the free energy for PMCA cycling was obtained from cytosolic Ca<sup>2+</sup> concentration with Fluo-3, which was calibrated with Mn<sup>2+</sup> as described in Materials and Methods. These three ions bear most of the weight when calculating the electrochemical potentials involved in ion pumping. Membrane potential and intracellular [H<sup>+</sup>], the other two variables to be considered, were estimated in parallel experiments and introduced into the respective equations (see Materials and Methods). Note that typical ATP phosphorylation potentials in healthy cells are more negative than -14 kcal/mol. The results, illustrated in Figure 11, reveal a marked difference between the two pumps. Product of the rapid dissipation of the gradients of Na<sup>+</sup> and K<sup>+</sup>, the free energy required for Na<sup>+</sup>/K<sup>+</sup> pump cycling becomes progressively smaller. In contrast, the free energy required for PMCA cycling remained constant in injured cells, because the large Ca<sup>2+</sup> gradient that characterizes viable cells remains almost intact even during the first minutes of the delayed Ca<sup>2+</sup> overload, so that the slight increase in cytosolic Ca<sup>2+</sup> was roughly cancelled out by the increase in [H<sup>+</sup>]. As a result, after 20–30 min peroxide exposure, the curves intercept (arrow in Figure 11), defining two periods of injury progression. In the first period, before the intercept, a putative drop in ATP concentration will first inhibit the Na<sup>+</sup> pump and then the Ca<sup>2+</sup> pump. During this first period, a fall in cell energy charge that is severe enough to inhibit the PMCA will also stop the Na<sup>+</sup>/K<sup>+</sup> pump. This makes

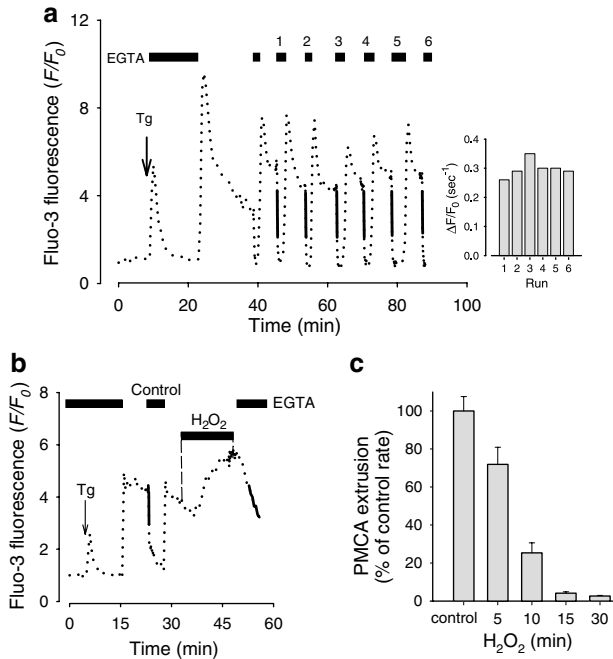


**Figure 7** Delayed PMCA failure during oxidative stress in HeLa cells. Cytosolic Ca<sup>2+</sup> fluorescence was estimated with Fluo-3 as described in Materials and Methods. (a) A cell was depleted of stored calcium with 5  $\mu$ M thapsigargin in the absence of extracellular Ca<sup>2+</sup> (10 mM EGTA). Re-exposure to Ca<sup>2+</sup> results in a steady state in which channel-mediated Ca<sup>2+</sup> entry is balanced by the PMCA. Upon chelation of extracellular Ca<sup>2+</sup>, the rapid deflection of the Fluo-3 signal corresponds to the rate of extrusion by the PMCA, a measurement that was reproduced six times with little variability (solid lines and bar graph). (b) PMCA activity was estimated before and after 15 min exposure to peroxide, showing a marked decrease in the rate of extrusion. (c) In experiments similar to that depicted in (b), the effect of increasing exposures to peroxide was assessed in more than three experiments for each time. Data are from 116, 46, 31, 37 and 49 cells for control, 5, 10, 15 and 30 min of peroxide exposure, respectively

it impossible for the Na<sup>+</sup> pump to outcompete the PMCA for ATP phosphorylation potential. In contrast, during the second period, from the intercept onwards, it becomes cheaper to pump Na<sup>+</sup>/K<sup>+</sup> than Ca<sup>2+</sup>/H<sup>+</sup>, so a drop in ATP will first inhibit the PMCA. Because Na<sup>+</sup> pumping can proceed at very low ATP phosphorylation potentials, for example,  $-4$  kcal/mol, it then becomes feasible for the Na<sup>+</sup>/K<sup>+</sup> pump to behave as a low ATP clamp. With energy charge below the minimum PMCA requirement, the Ca<sup>2+</sup> that enters the cell will not be extruded, leading to the delayed Ca<sup>2+</sup> overload. The effective reversal of PMCA inhibition and Ca<sup>2+</sup> overload afforded by ouabain and zero potassium strongly suggests that the mechanism keeping the energy charge below the PMCA requirement is indeed the Na<sup>+</sup>/K<sup>+</sup> pump, a phenomenon made possible by the severe Na<sup>+</sup> overload and K<sup>+</sup> depletion.

## Discussion

The main finding of this work is a novel sequence that involves Na<sup>+</sup> influx, Na<sup>+</sup>/K<sup>+</sup> pump activity, functional inhibition of the PMCA and Ca<sup>2+</sup> overload (Figure 12). This cascade provides a new mechanistic explanation for the permissive role of Na<sup>+</sup> in epithelial cell necrosis<sup>17,18</sup> and lengthens the growing list of

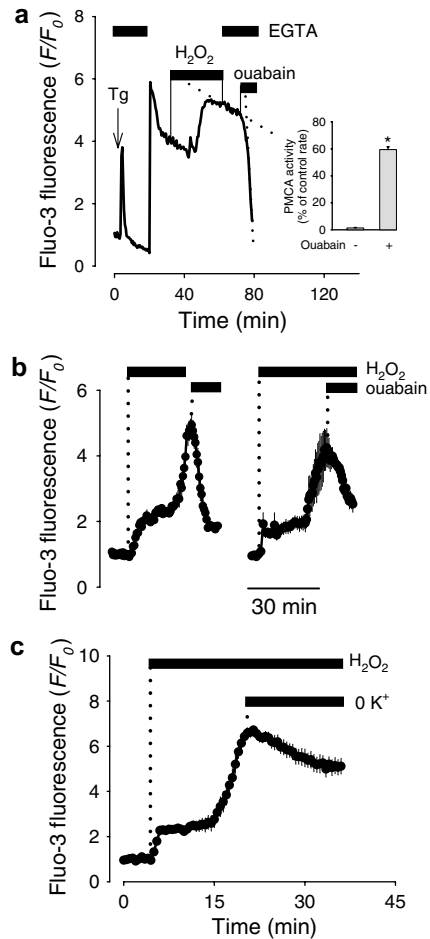


**Figure 8** Na<sup>+</sup>/K<sup>+</sup> pump inhibition rescues PMCA activity and reverts oxidative Ca<sup>2+</sup> overload in HeLa cells. Cytosolic Ca<sup>2+</sup> fluorescence was estimated with Fluo-3 as described in Materials and Methods. (a) After exposing a cell to peroxide for 30 min, PMCA activity was measured over 8 min. Next, 1 mM Ouabain was added, causing a sudden increase in the rate of Ca<sup>2+</sup> extrusion. The inset shows the data for 20 cells in two similar experiments, as a percentage of the rate measured in control cells. \* $P < 0.05$  with respect to the rate before ouabain. (b) The delayed calcium overload was reverted by 1 mM Ouabain both in the absence (left panel) and presence (right panel) of H<sub>2</sub>O<sub>2</sub>. (c) Removal of extracellular potassium also reverted the delayed Ca<sup>2+</sup> overload. For (b) and (c), similar data were obtained in three experiments of each kind

**Table 1** Na<sup>+</sup>/K<sup>+</sup> ATPase activity during oxidative stress in HeLa cells

<sup>86</sup> Rb uptake (nmol/mg protein)	H <sub>2</sub> O <sub>2</sub>		
	Control	15 min	30 min
Ouabain-sensitive	2.2 ± 0.3	1.0 ± 0.3	1.1 ± 0.2
Ouabain-insensitive	1.9 ± 0.2	1.7 ± 0.2	1.1 ± 0.1

Na<sup>+</sup> toxicity mechanisms (Sheldon *et al.*<sup>19</sup> and references therein). This mechanism differs from that in textbooks,<sup>20</sup> which pose the Ca<sup>2+</sup> overload downstream of reversed NCX or activated VOCCs.<sup>21</sup> However, the two pathways are not necessarily exclusive.

The sequence begins with increased Na<sup>+</sup> influx, which together with a moderate decrease in Na<sup>+</sup>/K<sup>+</sup> ATPase

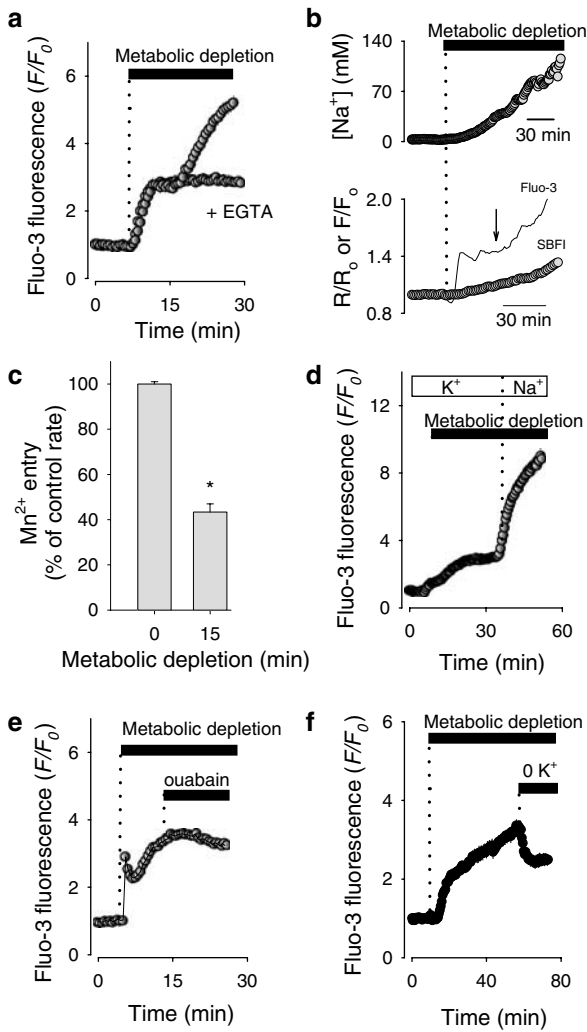


**Figure 9** The Na<sup>+</sup>/K<sup>+</sup> pump also participates in the delayed Ca<sup>2+</sup> overload induced by metabolic depletion in HeLa cells. Cytosolic Ca<sup>2+</sup> and Na<sup>+</sup> were estimated with Fluo-3 and SBF1 respectively and Mn<sup>2+</sup> entry rate was estimated by calcein quenching (Materials and Methods). (a) Metabolic depletion, as induced with 500 μM iodoacetate, 5 mM deoxyglucose and 1 μM antimycin A, caused a biphasic increase in cytosolic Ca<sup>2+</sup> (closed symbols). In the absence of extracellular Ca<sup>2+</sup> (10 mM EGTA), only the early phase was observed (open symbols). Data are representative of seven experiments. (b) Na<sup>+</sup> overload in response to metabolic inhibition (top panel). The lower panel shows that in cells co-loaded with SBF1 and Fluo-3, Na<sup>+</sup> began to increase simultaneously with the early Ca<sup>2+</sup> rise and before the onset of the delayed Ca<sup>2+</sup> rise (arrow). Similar data were obtained in three other experiments. (c) The rate of Mn<sup>2+</sup> entry was measured before and after 15 min of metabolic depletion. Data are from two experiments. (d) The delayed Ca<sup>2+</sup> overload, not observed in the absence of extracellular Na<sup>+</sup> is triggered by its re-addition. Data are representative of three experiments. The delayed Ca<sup>2+</sup> overload was reverted with 1 mM ouabain (e) or withdrawal of extracellular potassium (f). Similar results were obtained in three experiments for each protocol

activity leads to Na<sup>+</sup> overload and swelling. By 60 min, intracellular [Na<sup>+</sup>] has reached the extracellular level but cells have swollen by only 25%, witnessing a sizable loss of K<sup>+</sup>. The mechanism of this K<sup>+</sup> loss is currently under investigation. The molecular mechanism of the Na<sup>+</sup> influx is also beyond the scope of the present report, but the dissociation observed between Ca<sup>2+</sup> entry and Na<sup>+</sup> entry suggests that the pathway responsible for the latter is monovalent-selective.

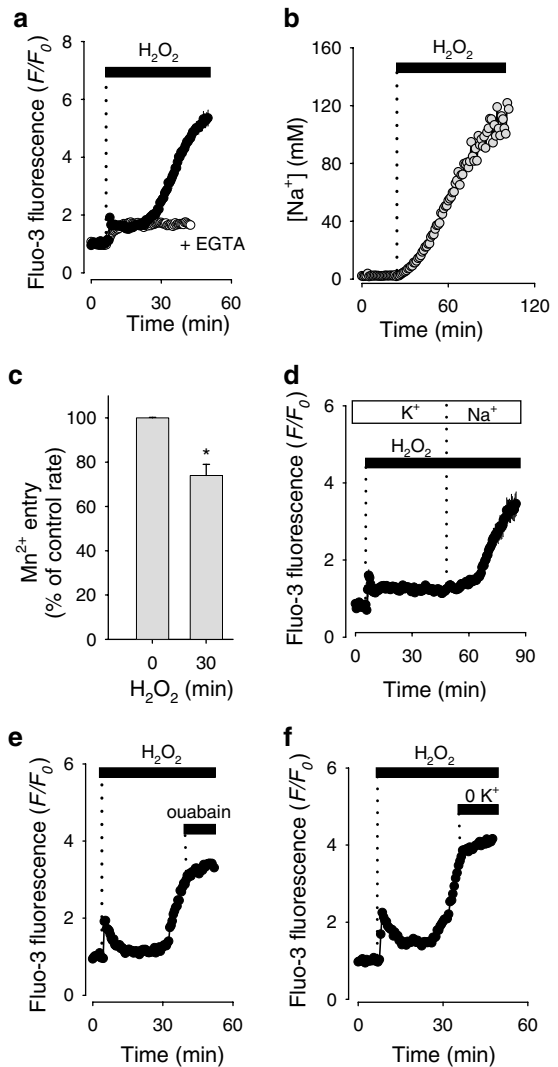


**Figure 10** The Na<sup>+</sup>/K<sup>+</sup> pump participates in the delayed Ca<sup>2+</sup> overload in MDCK cells. Cytosolic Ca<sup>2+</sup> and Na<sup>+</sup> fluorescence were estimated with Fluo-3 and SBF1, respectively, and Mn<sup>2+</sup> entry rate was estimated by calcein quenching (Materials and Methods). (a) Hydrogen peroxide caused a biphasic increase in cytosolic Ca<sup>2+</sup> (closed symbols). In the absence of extracellular Ca<sup>2+</sup> (EGTA), only the early phase was observed (open symbols). Data are representative of four experiments. (b) Na<sup>+</sup> overload in response to peroxide. Similar data were obtained in three other experiments. (c) The rate of Mn<sup>2+</sup> entry was measured before and after 30 min of peroxide exposure. Data are from two experiments. (d) The delayed Ca<sup>2+</sup> overload, not observed in the absence of extracellular Na<sup>+</sup> was triggered after its re-addition. Data are representative of three experiments. The delayed Ca<sup>2+</sup> overload was reverted with 1 mM ouabain (e) or withdrawal of extracellular potassium (f). Similar results were obtained in three experiments for each protocol

We know from previous work in epithelial cells that prime candidates are the Na<sup>+</sup>/H<sup>+</sup> exchanger, Na<sup>+</sup> channels and monovalent-selective cation channels.<sup>4,17,18,22</sup> While Na<sup>+</sup> was still rising, cytosolic Ca<sup>2+</sup> stabilized at about two-fold the initial value, owing to a dynamic balance between decreased buffer capacity,<sup>7</sup> decreased entry and decreased extrusion. Initially, the steady state was robust, as evidenced by its response to perturbation (Figure 6), but 20–40 min later, the steady state was broken and Ca<sup>2+</sup> rose again, this time in a

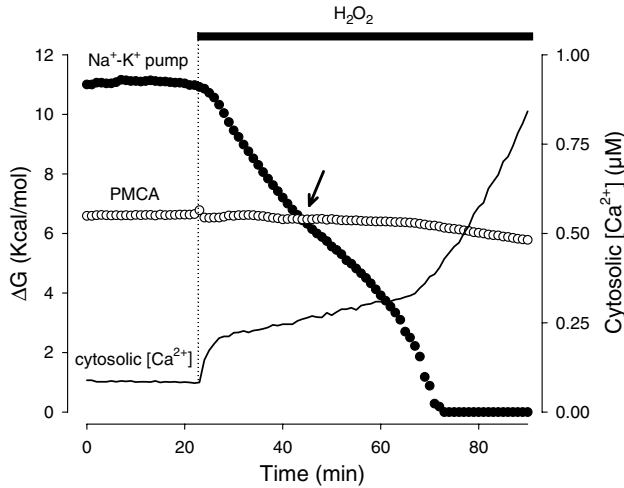


**Figure 11** Thermodynamic dissociation of Na<sup>+</sup>/K<sup>+</sup> pumping and PMCA pumping during oxidative stress in HeLa cells. The free energies involved in Na<sup>+</sup>/K<sup>+</sup> pumping (closed symbols) and PMCA cycling (open symbols) were calculated from measured ion concentrations as explained in Materials and Methods. The continuous line represents cytosolic [Ca<sup>2+</sup>]. Data are from eight cells. Note that in this experiment, Na<sup>+</sup>/K<sup>+</sup> pumping became more economic than Ca<sup>2+</sup>/H<sup>+</sup> exchange 27 min after injury onset (arrow). In other three similar experiments, the intersection occurred at 23, 26 and 27 min

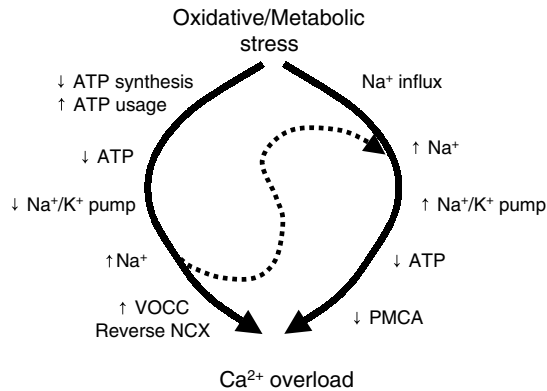


**Figure 12** Pathways of necrotic Ca<sup>2+</sup> overload. The canonical sequence (left) involves a primary deficit in ATP synthesis that leads to Na<sup>+</sup>/K<sup>+</sup> pump inhibition and thus Na<sup>+</sup> accumulation. The latter results in increased Ca<sup>2+</sup> influx via channels or transporters. ATP steal (right) ensues when injury-resilient Na<sup>+</sup>/K<sup>+</sup> pumps deplete the vicinity of the PMCA of phosphorylation potential. As this residual Na<sup>+</sup>/K<sup>+</sup> pump activity may also be caused by Na<sup>+</sup> accumulation/K<sup>+</sup> depletion secondary to Na<sup>+</sup>/K<sup>+</sup> pump inhibition, the two pathways may be linked (dotted line)

sustained fashion. The onset of the second phase coincided with necrotic commitment. As demonstrated by its sensitivity to gadolinium and extracellular Ca<sup>2+</sup> chelation, the source of this Ca<sup>2+</sup> rise was the extracellular space and not the endoplasmic reticulum, the mitochondria or other intracellular stores.<sup>23–25</sup> Surprisingly, Ca<sup>2+</sup> permeability during stress was found to be lower than control, ruling out a significant role for newly activated surface Ca<sup>2+</sup> channels or reverse NCXs. The underlying mechanism was clarified when PMCA activity was found to collapse approaching the onset of the Ca<sup>2+</sup> rise. Thus, Ca<sup>2+</sup> rose in the face of reduced Ca<sup>2+</sup> entry because Ca<sup>2+</sup> extrusion decreased to an even larger extent. Inciden-

tally, reduced Ca<sup>2+</sup> permeability has also been reported in hypoxic kidney tubules, where it was ascribed a protective role.<sup>26</sup> In contrast to the permanent inactivation of the PMCA by thiol modification<sup>27</sup> or proteolytic cleavage,<sup>11</sup> the fall in PMCA activity early during stress was reversible. Resistance of the PMCA and other Ca<sup>2+</sup> pumps to hydrogen peroxide has been reported earlier,<sup>25,28</sup> which for the PMCA is conferred by calmodulin.<sup>29</sup> As the functional inhibition of the PMCA was abolished in the absence of Na<sup>+</sup>, in the absence of extracellular K<sup>+</sup> or in the presence of ouabain, it was concluded that PMCA inhibition required Na<sup>+</sup>/K<sup>+</sup> pump activity. In accordance with a key role for Na<sup>+</sup>/K<sup>+</sup> pump-mediated PMCA inhibition in the progression of the delayed Ca<sup>2+</sup> overload, blockage of the Na<sup>+</sup>/K<sup>+</sup> pump also protected against necrosis. In addition to the observed decrease in Ca<sup>2+</sup> permeability, a putative role for reverse Na<sup>+</sup>/Ca<sup>2+</sup> exchange in the Ca<sup>2+</sup> overload was discarded, as the Ca<sup>2+</sup> rise was inhibited instead of being stimulated by rapid extracellular Na<sup>+</sup> removal.

Other than the cascades illustrated in Figure 12, Ca<sup>2+</sup> overload may result from the activation of Ca<sup>2+</sup>-permeable channels, some of which have been characterized at the molecular level.<sup>9,10,30</sup> Our data do not rule out a role for these channels at later stages of epithelial necrosis, but suggest that they are not relevant for its onset, at least in the cell types and conditions presented here. The same can be said for intracellular Ca<sup>2+</sup> sources such as mitochondria<sup>23</sup> and endoplasmic reticulum.<sup>24,25</sup>

In the absence of evidence for direct interaction between the Na<sup>+</sup>/K<sup>+</sup> pump and the PMCA, we speculate that metabolic crosstalk is the most economical hypothesis to account for our data. With the caveat that fluorescence measurements do not provide information on local ion concentrations, a calculation of the free energies involved in pumping shows that in healthy cells, a sudden fall in energy charge would always starve the Na<sup>+</sup> pump before the PMCA (Figure 11). This is true even if energy depletion were due to the activity of the Na<sup>+</sup> pump itself, for its ATPase activity will cease at ATP phosphorylation potentials less negative than –10 kcal/mol. For instance, at –4 kcal/mol, both pumps will be fully inhibited or reversed. Different however is the situation in Na<sup>+</sup>-loaded cells, where the energy required to sustain Na<sup>+</sup> pumping decreases considerably. For instance, in the experiment depicted in Figure 11, if after 60 min of injury the ATP phosphorylation potential were –4 kcal/mol, the Na<sup>+</sup> pump would still be cycling (and using ATP), whereas the PMCA would have stopped or even reversed, becoming an ATP source. Information on the ATP hydrolysis potential in the vicinity of the ion pumps is not available, but it appears that at the onset of the Ca<sup>2+</sup> overload, it must be less negative than the –6 kcal/mol required by the PMCA. Thus, it appears likely that the Na<sup>+</sup>/K<sup>+</sup> pump inhibition by ouabain or K<sup>+</sup> removal increases the local availability of ATP phosphorylation potential, causing the PMCA to restart and revert the overload. This phenomenon bears some analogy to the subclavian ‘flow steal’ syndrome, a clinical condition in which a stenosis proximal to the branching of the vertebral artery allows the exercising arm to ‘steal’ blood flow from the brain by virtue of its lower input resistance (i.e. lower free energy). For this reason, we have used the term ‘ATP steal’ for the

metabolic crosstalk between ion pumps during stress. An attractive feature of ATP steal is that it explains the permissive role of Na<sup>+</sup> in epithelial cell necrosis without reference to NCX or VOCC, proteins that are scarce in non-excitabile cells. Even in excitable cells, NCX and VOCC may play a less important pathogenic role than once thought.<sup>19,31</sup>

Owing to its inhibition of glycolysis and oxidative phosphorylation plus activation of ATP usage by poly (ADP ribose) polymerase, hydrogen peroxide causes severe ATP depletion.<sup>3,32–34</sup> A role for the Na<sup>+</sup>/K<sup>+</sup> ATPase as a significant ATP sink in H<sub>2</sub>O<sub>2</sub>-exposed cells was previously discarded in endothelial cells based on the failure of ouabain to rescue the ATP depletion.<sup>35</sup> Using HeLa-LUC, a cell line permanently transfected with firefly luciferase, we have confirmed that after 30 min of oxidative or metabolic inhibition, bulk ATP levels are very low<sup>12</sup> and that the ATP depletion is refractory to the addition of ouabain (I Ruminot *et al.*, unpublished data). However, at that time, there remains a surprisingly high Na<sup>+</sup>/K<sup>+</sup> ATPase activity (50% of control). Moreover, ouabain was able to unveil a robust PMCA activity (60% of control). It follows that a local source of ATP is readily available to the pumps with little incidence on bulk ATP, a source that in Na<sup>+</sup>-loaded cells is monopolized by the Na<sup>+</sup>/K<sup>+</sup> pump to the detriment of the PMCA. This contention appears reasonable in light of existing evidence for the presence of a membrane-associated ATP pool and the preferential delivery of glycolytic ATP to both cation pumps.<sup>36–38</sup>

In this study, the delayed Ca<sup>2+</sup> overload was elicited in HeLa cells by two different protocols. The Ca<sup>2+</sup> overload was also studied in MDCK cells. In all cases, overload onset responded to the same basic mechanism. In addition, a previous report suggests that ATP steal may not be restricted to epithelial cells. On studying the effect of an imposed Na<sup>+</sup> load over synaptosomes stressed with hydrogen peroxide, a Ca<sup>2+</sup> overload was observed that shares several features with that observed in HeLa cells and MDCK cells, requiring both extracellular Ca<sup>2+</sup> and Na<sup>+</sup>. Although the synaptosome study did not include measurement of Ca<sup>2+</sup> permeability or cation pump activity, and a role for reverse NCX could not be ruled out, the Ca<sup>2+</sup> rise was significantly attenuated by ouabain, implying a possible role for the Na<sup>+</sup> pump.<sup>39</sup> Another possible non-epithelial example of ATP steal may occur in vascular endothelial cells, for tert-butyl hydroperoxide induced both an irreversible increase in cytosolic Ca<sup>2+</sup><sup>40</sup> and an increase in Na<sup>+</sup>/K<sup>+</sup> pump activity.<sup>41</sup>

## Materials and Methods

### Chemicals

Fluorescence dyes and pluronic acid were purchased from Molecular Probes (Eugene, OR, USA). Hydrogen peroxide was from Merck (Darmstadt, Germany). Ca<sup>2+</sup> 45 (2 Ci/mmol) Radionuclide (<sup>45</sup>Ca<sup>2+</sup>) was purchased from DuPont-New England Nuclear. The Micro BCA™ Protein Assay Kit was from PIERCE (Rockford, IL, USA). Tissue culture reagents and chemicals were from Sigma (St. Louis, MO, USA).

### Cell culture and viability measurements

HeLa cells, a human epithelial cell line, and MDCK, a canine epithelial cell line, were obtained from the American Tissue Culture Collection Cells, and

cultured in Dulbecco's modified Eagle's medium supplemented with 7% fetal calf serum, at 37°C in a humidified atmosphere of 5% CO<sub>2</sub> and 95% air. Cells between passage numbers 8 and 30 were exposed to experimental conditions in Krebs–Ringer–Hepes buffer (KRH; 136 mM NaCl, 10 mM Hepes, 4.7 mM KCl, 1.25 mM MgSO<sub>4</sub>, 1.25 mM CaCl<sub>2</sub>, pH 7.4) supplemented with 25 mM glucose (KRH-glc). In selected experiments, Na<sup>+</sup> was replaced equimolarly by *N*-methyl-D-glucamine (NMDG<sup>+</sup>), K<sup>+</sup> or Cs<sup>+</sup>, whereas in others, Ca<sup>2+</sup> was chelated by addition of 10 mM EGTA. In selected experiments, the cells were exposed to experimental conditions in Ca<sup>2+</sup>-free medium (KRH-glc without CaCl<sub>2</sub> plus 500 μM EGTA). LDH, which is released during cell necrosis, was determined in cell supernatants by a colorimetric end point kit from Wiener Laboratory (Rosario, Argentina); results are expressed as percentage of maximum release, measured in the presence of 100 μM digitonin.

### Measurement of cell volume by three-dimensional reconstruction

HeLa cells were transferred to microscopic four-well culture chambers (Nalge Nunc, Rochester, NY, USA) and incubated for 24–48 h before the experiments. Plasma membranes cells were stained for 30 min at 37°C with 3 μM DiIc18. Three-dimensional stacks were captured at room temperature (22–24°C) in KRH-glc with an LSM 5 Pascal Zeiss confocal inverted microscope (× 63 water-immersion objective, NA 1.2, excitation 543 nm/emission 560–615 nm, voxel dimensions (μm)  $x = 0.286$ ,  $y = 0.286$ ,  $z \leq 1.2$ , voxel unit volume  $\leq 0.1 \mu\text{m}^3$ ). In control experiments, we observed that vertical sampling distances shorter than 1.2 μm did not improve the reliability of volume measurements (data not shown). In additional control experiments, cell volumes fluctuated less than ~3% (standard deviation) over a 1 h period with sampling every 5 min. The signal to noise ratio of the images was improved by deconvolution with Huygens Professional (Scientific Volume Imaging BV, Hilversum, The Netherlands). All image processing routines for further analysis were written in IDL (Research Systems, CO, USA). First, segmentation of the cells from the background was achieved by fixing threshold values in the intensity histogram of the images. False positive regions and remaining holes were corrected by morphological filters based on region size. Remaining heterogeneities of the automated segmentation were corrected manually (PhotoStudio, ArcSoft Inc., www.arcsoft.com). Cellular volume was calculated by multiplying the unit voxel volume by the total number of segmented voxels.

### Fluorescence measurements

All experiments were carried out at room temperature (22–24°C). Confocal epifluorescence microscopy was carried out with an LSM 5 Pascal Zeiss confocal microscope. Fluo-3 and calcein were imaged at 488 nm excitation/505–550 nm emission, and PI was imaged at 543 nm excitation/560–615 nm emission. Simultaneous imaging of SBFI (340/380 nm excitation/510–560 nm emission) and Fluo-3 (485 nm excitation/510–560 nm emission) was with an Olympus IX70 microscope equipped with a Cairn monochromator (Faversham, UK) and a Hamamatsu Orca camera (Hamamatsu city, Japan). Dyes were ester-loaded at 5 μM for 30 min at room temperature in KRH-glc containing 0.02% pluronic. De-esterification period was 30 min. Oxonol, a negatively charged membrane-permeable dye that loads in a manner proportional to membrane potential,<sup>42</sup> was equilibrated with the cells for 30 min at 4 μM before imaging by confocal microscopy (543 excitation/ > 585 nm emission). For all dyes, the average fluorescence value of regions of interest positioned

on the nuclei was registered every 20–30 s. At these time intervals, nuclear and cytosolic ion concentrations are at equilibrium in HeLa cells. SBF1 calibration was carried out by exposing cells permeabilized with 20 µg/ml gramicidin to KRH-glc, which had their Na<sup>+</sup> replaced in eight different proportions by K<sup>+</sup>.  $K_D$ 's fluctuated between 40 and 45 mM as reported earlier<sup>43</sup> and were not affected by mM H<sub>2</sub>O<sub>2</sub>. To quantify Ca<sup>2+</sup> using Fluo-3, the dye was calibrated with Mn<sup>2+</sup> in ionomycin-treated cells, as described.<sup>44</sup>

### Cation permeability assays

To measure Na<sup>+</sup> permeability, SBF1-loaded cells were preincubated for 30 min in KRH buffers in which Na<sup>+</sup> had been replaced by NMDG<sup>+</sup> or K<sup>+</sup>, in the presence of 1 mM ouabain. After exposure to experimental conditions, the buffer was changed to 1 mM ouabain in KRH and SBF1 was imaged as detailed above. Initial rates were obtained from the first derivative of a two-parameter exponential fitted to the time courses by nonlinear regression. To measure Ca<sup>2+</sup> permeability, cells grown in six-well culture plates were exposed to <sup>45</sup>Ca<sup>2+</sup> 5 µCi in KRH-glc with no added Ca<sup>2+</sup> for 30 min. Next, cells were washed three times with ice-cold PBS and the tracer was released with 1% of Triton, dissolved in scintillation fluid and quantified in a Berthold Luminometer (Pforzheim, Germany). Total soluble protein content per dishes was estimated by the bicinchoninic acid method. <sup>45</sup>Ca<sup>2+</sup> uptake was expressed as c.p.m./mg protein in each dish. Membrane permeability to divalents was assessed using a Mn<sup>2+</sup> quenching technique, modified from Hallam and Rink.<sup>45</sup> Briefly, after loading the cells with calcein, the entry of 5 mM MnCl<sub>2</sub> was monitored by the progressive quenching of the dye. Rates were obtained by fitting a linear function to the initial part of the quenching curve using minimum squares.

### Assessment of PMCA activity

Two independent methods were used to estimate the capability of cells to extrude Ca<sup>2+</sup>. Firstly, a rapid increase in cytosolic Ca<sup>2+</sup> was induced in Fluo-3-loaded cells by mechanical stimulation with a blunt-ended glass micropipette (a 2 s touch) using an automated Eppendorf micromanipulator (Hamburg, Germany). Recovery to basal values was then monitored by confocal microscopy. Secondly, PMCA activity was quantified in Fluo-3-loaded cells using the protocol described by Klishin *et al.*<sup>15</sup> Intracellular Ca<sup>2+</sup> stores were first emptied with 5 µM thapsigargin in the absence of extracellular Ca<sup>2+</sup>, which leads to the activation of store operated Ca<sup>2+</sup> channels (SOCs). Re-application of Ca<sup>2+</sup> induces a sustained influx of the divalent through SOCs, with cytosolic Ca<sup>2+</sup> reaching a new steady state when the activated PMCA matches the rate of entry. At this point, quick chelation of extracellular Ca<sup>2+</sup> with 10 mM EGTA stops the entry, causing a fall in cytosolic Ca<sup>2+</sup> whose rate corresponds to that of PMCA extrusion. Rates were compared in the same range of Fluo-3 fluorescence.

### Assessment of Na<sup>+</sup>/K<sup>+</sup> pump activity

Na<sup>+</sup>/K<sup>+</sup> pump activity was determined at room temperature by measuring ouabain-sensitive <sup>86</sup>Rb<sup>+</sup>/K<sup>+</sup> uptake as detailed previously.<sup>46</sup> HeLa cells were grown at 80% confluency in 24-well plastic plates (Sarstedt, Germany). Before the uptake assay, cells were preincubated for 10 min in KRH and then with 32 mM H<sub>2</sub>O<sub>2</sub> in KRH for 15 or 30 min. Ouabain (1 mM) was added during the last 3 min of incubation and then the uptake assay was launched by addition of <sup>86</sup>Rb<sup>+</sup> (1 µCi/ml; 2–7 µM). After 7 min of uptake, extracellular radioactivity was removed by washing

thrice with ice-cold KRH. Control experiments showed that ouabain-sensitive uptake is linear for at least 12 min under these conditions. Radioactivity was extracted with 0.2 N NaOH for 2 h, neutralized with HCl and counted with a Packard Tricarb liquid scintillation analyzer (model 1600 TR).

### Calculation of electrochemical potentials

The free energies required by the Na<sup>+</sup>/K<sup>+</sup> pump ( $\Delta G_{Na^+/K^+ \text{ pump}}$ ) and by the PMCA ( $\Delta G_{PMCA}$ ) were calculated with the equations

$$\Delta G_{Na^+/K^+ \text{ pump}} = 3RT \ln([Na^+]_i/[Na^+]_e) + 2RT \ln([K^+]_e/[K^+]_i) + F \Delta V$$

$$\Delta G_{PMCA} = RT \ln([Ca^{2+}]_i/[Ca^{2+}]_e) + RT \ln([H^+]_e/[H^+]_i) + F \Delta V$$

where  $R$  is the gas constant (1.987 cal/mol/deg),  $T$  is the temperature in Kelvin degrees (296 K),  $F$  is Faraday's constant (23 062 cal/V/mol) and  $\Delta V$  is the cell's membrane potential.  $[Na^+]_i$ ,  $[K^+]_i$  and  $[Ca^{2+}]_i$  were measured simultaneously using SBF1 and Fluo3, as described above.  $[H^+]_i$  and  $\Delta V$  were estimated in parallel experiments using BCECF<sup>7</sup> and oxonol,<sup>42</sup> respectively.

### Statistical analysis

Data are presented as means  $\pm$  S.E.M. (8–10 cells) unless otherwise stated. In some cases, the errors were smaller than the symbols. Regression analyses were performed with SigmaPlot (Jandel Corp.). Statistical significance was assessed using Student's  $t$ -test to compare two samples. Differences between means were considered significant at  $P < 0.05$ .

### Acknowledgements

IR, CF and EV are students at the Universidad Austral de Chile. We thank Karen Everett for critical reading of the manuscript. This work was funded by Fondecyt Grants 1020648 and 1051082 (to LFB), 1050690 (to LM) and 3030065 (to SH). The Centro de Estudios Científicos (CECS) receives institutional support from Empresas CMPC, the Millenium Science Initiative, Fundación Andes and the Tinker Foundation.

### References

1. Majno G and Joris I (1995) Apoptosis, oncosis, and necrosis. An overview of cell death. *Am. J. Pathol.* 146: 3–15
2. Zahrebelski G, Nieminen AL, al Ghoul K, Qian T, Herman B and Lemasters JJ (1995) Progression of subcellular changes during chemical hypoxia to cultured rat hepatocytes: a laser scanning confocal microscopic study. *Hepatology* 21: 1361–1372
3. Ha HC and Snyder SH (1999) Poly(ADP-ribose) polymerase is a mediator of necrotic cell death by ATP depletion. *Proc. Natl. Acad. Sci. USA* 96: 13978–13982
4. Barros LF, Hermosilla T and Castro J (2001) Necrotic volume increase and the early physiology of necrosis. *Comp. Biochem. Physiol. A* 130: 401–409
5. Lee JM, Zipfel GJ and Choi DW (1999) The changing landscape of ischaemic brain injury mechanisms. *Nature* 399: A7–A14
6. Ermak G and Davies KJ (2002) Calcium and oxidative stress: from cell signaling to cell death. *Mol. Immunol.* 38: 713–721

7. Castro J, Bittner CX, Humeres A, Montecinos VP, Vera JC and Barros LF (2004) A cytosolic source of calcium unveiled by hydrogen peroxide with relevance for epithelial cell death. *Cell Death Differ.* 11: 468–478
8. Herson PS, Lee K, Pinnock RD, Hughes J and Ashford ML (1999) Hydrogen peroxide induces intracellular calcium overload by activation of a non-selective cation channel in an insulin-secreting cell line. *J. Biol. Chem.* 274: 833–841
9. Aarts M, Iihara K, Wei WL, Xiong ZG, Arundine M, Cerwinski W, MacDonald JF and Tymianski M (2003) A key role for TRPM7 channels in anoxic neuronal death. *Cell* 115: 863–877
10. Xiong ZG, Zhu XM, Chu XP, Minami M, Hey J, Wei WL, MacDonald JF, Wemmie JA, Price MP, Welsh MJ and Simon RP (2004) Neuroprotection in ischemia: blocking calcium-permeable acid-sensing ion channels. *Cell* 118: 687–698
11. Schwab BL, Guerini D, Didszun C, Bano D, Ferrando-May E, Fava E, Tam J, Xu D, Xanthoudakis S, Nicholson DW, Carafoli E and Nicotera P (2002) Cleavage of plasma membrane calcium pumps by caspases: a link between apoptosis and necrosis. *Cell Death Differ.* 9: 818–831
12. Barros LF, Kanaseki T, Sabirov R, Morishima S, Castro J, Bittner CX, Maeno E, Ando-akatsuka Y and Okada Y (2003) Apoptotic and necrotic blebs in epithelial cells display similar neck diameters but different kinase dependency. *Cell Death Differ.* 10: 687–697
13. Bortner CD and Cidlowski JA (2002) Cellular mechanisms for the repression of apoptosis. *Annu. Rev. Pharmacol. Toxicol.* 42: 259–281
14. Barros LF, Castro J and Bittner CX (2002) Ion movements in cell death: from protection to execution. *Biol. Res.* 35: 209–214
15. Klishin A, Sedova M and Blatter LA (1998) Time-dependent modulation of capacitative Ca<sup>2+</sup> entry signals by plasma membrane Ca<sup>2+</sup> pump in endothelium. *Am. J. Physiol.* 274: C1117–C1128
16. Bortner CD and Cidlowski JA (2003) Uncoupling cell shrinkage from apoptosis reveals that Na<sup>+</sup> influx is required for volume loss during programmed cell death. *J. Biol. Chem.* 278: 39176–39184
17. Carini R, Bellomo G, Benedetti A, Fulceri R, Gamberucci A, Parola M, Dianzani MU and Albano E (1995) Alteration of Na<sup>+</sup> homeostasis as a critical step in the development of irreversible hepatocyte injury after adenosine triphosphate depletion. *Hepatology* 21: 1089–1098
18. Barros LF, Stutzin A, Calixto A, Catalán M, Castro J, Hetz C and Hermosilla T (2001) Non-selective cation channels as effectors of free radical-induced rat liver cell necrosis. *Hepatology* 33: 114–122
19. Sheldon C, Diarra A, Cheng YM and Church J (2004) Sodium influx pathways during and after anoxia in rat hippocampal neurons. *J. Neurosci.* 24: 11057–11069
20. Greger R (2000) Membrane voltage and preservation of the ionic distribution across the cell membrane. In *Comprehensive Human Physiology*, Greger R, Windhurst U, eds (Berlin Germany: Springer-Verlag) Chapter 11, pp. 245–266
21. Yu SP (2003) Na(+), K(+)-ATPase: the new face of an old player in pathogenesis and apoptotic/hybrid cell death. *Biochem. Pharmacol.* 66: 1601–1609
22. Simon F, Varela D, Eguiguren AL, Diaz LF, Sala F and Stutzin A (2004) Hydroxyl radical activation of a Ca(2+)-sensitive nonselective cation channel involved in epithelial cell necrosis. *Am. J. Physiol. Cell Physiol.* 287: C963–C970
23. Wang H and Joseph JA (2000) Mechanisms of hydrogen peroxide-induced calcium dysregulation in PC12 cells. *Free Radic. Biol. Med.* 28: 1222–1231
24. Xu K, Tavernarakis N and Driscoll M (2001) Necrotic cell death in *C. elegans* requires the function of calreticulin and regulators of Ca(2+) release from the endoplasmic reticulum. *Neuron* 31: 957–971
25. Favero TG, Zable AC and Abramson JJ (1995) Hydrogen peroxide stimulates the Ca<sup>2+</sup> release channel from skeletal muscle sarcoplasmic reticulum. *J. Biol. Chem.* 270: 25557–25563
26. Peters SM, Tijssen MJ, van Os CH, Wetzels JF and Bindels RJ (1998) Hypoxia decreases calcium influx into rat proximal tubules. *Kidney Int.* 53: 703–708
27. Nicotera P, Hartzell P, Baldi C, Svensson SA, Bellomo G and Orrenius S (1986) Cystamine induces toxicity in hepatocytes through the elevation of cytosolic Ca<sup>2+</sup> and the stimulation of a nonlysosomal proteolytic system. *J. Biol. Chem.* 261: 14628–14635
28. Zaidi A and Michaelis ML (1999) Effects of reactive oxygen species on brain synaptic plasma membrane Ca(2+)-ATPase. *Free Radic. Biol. Med.* 27: 810–821
29. Zaidi A, Barron L, Sharov VS, Schoneich C, Michaelis EK and Michaelis ML (2003) Oxidative inactivation of purified plasma membrane Ca<sup>2+</sup>-ATPase by hydrogen peroxide and protection by calmodulin. *Biochemistry* 42: 12001–12010
30. Bianchi L, Gerstbrein B, Frokjaer-Jensen C, Royal DC, Mukherjee G, Royal MA, Xue J, Schafer WR and Driscoll M (2004) The neurotoxic MEC-4(d) DEG/ENaC sodium channel conducts calcium: implications for necrosis initiation. *Nat. Neurosci.* 7: 1337–1344
31. Mochizuki S and MacLeod KT (1997) Effects of hypoxia and metabolic inhibition on increases in intracellular Ca<sup>2+</sup> concentration induced by Na<sup>+</sup>/Ca<sup>2+</sup> exchange in isolated guinea-pig cardiac myocytes. *J. Mol. Cell. Cardiol.* 29: 2979–2987
32. Schraufstatter IU, Hyslop PA, Hinshaw DB, Spragg RG, Sklar LA and Cochrane CG (1986) Hydrogen peroxide-induced injury of cells and its prevention by inhibitors of poly(ADP-ribose) polymerase. *Proc. Natl. Acad. Sci. USA* 83: 4908–4912
33. Hyslop PA, Hinshaw DB, Halsey Jr WA, Schraufstatter IU, Sauerheber RD, Spragg RG, Jackson JH and Cochrane CG (1988) Mechanisms of oxidant-mediated cell injury. The glycolytic and mitochondrial pathways of ADP phosphorylation are major intracellular targets inactivated by hydrogen peroxide. *J. Biol. Chem.* 263: 1665–1675
34. Colussi C, Albertini MC, Coppola S, Rovidati S, Galli F and Ghibelli L (2000) H<sub>2</sub>O<sub>2</sub>-induced block of glycolysis as an active ADP-ribosylation reaction protecting cells from apoptosis. *FASEB J.* 14: 2266–2276
35. Spragg RG, Hinshaw DB, Hyslop PA, Schraufstatter IU and Cochrane CG (1985) Alterations in adenosine triphosphate and energy charge in cultured endothelial and P388D1 cells after oxidant injury. *J. Clin. Invest.* 76: 1471–1476
36. Fossel ET and Solomon AK (1978) Ouabain-sensitive interaction between human red cell membrane and glycolytic enzyme complex in cytosol. *Biochim. Biophys. Acta* 510: 99–111
37. Mercer RW and Dunham PB (1981) Membrane-bound ATP fuels the Na/K pump. Studies on membrane-bound glycolytic enzymes on inside-out vesicles from human red cell membranes. *J. Gen. Physiol.* 78: 547–568
38. Hardin CD, Raeymaekers L and Paul RJ (1992) Comparison of endogenous and exogenous sources of ATP in fueling Ca<sup>2+</sup> uptake in smooth muscle plasma membrane vesicles. *J. Gen. Physiol.* 99: 21–40
39. Chinopoulos C, Tretter L, Rozsa A and Adam-Vizi V (2000) Exacerbated responses to oxidative stress by an Na(+) load in isolated nerve terminals: the role of ATP depletion and rise of [Ca(2+)](i). *J. Neurosci.* 20: 2094–2103
40. Elliott SJ, Eskin SG and Schilling WP (1989) Effect of t-butyl-hydroperoxide on bradykinin-stimulated changes in cytosolic calcium in vascular endothelial cells. *J. Biol. Chem.* 264: 3806–3810
41. Elliott SJ and Schilling WP (1992) Oxidant stress alters Na<sup>+</sup> pump and Na(+)-K(+)-Cl<sup>-</sup> cotransporter activities in vascular endothelial cells. *Am. J. Physiol.* 263: H96–H102
42. Reyes JG, Bacigalupo J, Araya R and Benos DJ (1994) Ion dependence of resting membrane potential of rat spermatids. *J. Reprod. Fertil.* 102: 313–319
43. Diarra A, Sheldon C and Church J (2001) *In situ* calibration and [H<sup>+</sup>] sensitivity of the fluorescent Na<sup>+</sup> indicator SBFI. *Am. J. Physiol. Cell Physiol.* 280: C1623–C1633
44. Nadal A, Fuentes E and McNaughton PA (1996) Albumin stimulates uptake of calcium into subcellular stores in rat cortical astrocytes. *J. Physiol. (London)*. 492: 737–750
45. Hallam TJ and Rink TJ (1985) Agonists stimulate divalent cation channels in the plasma membrane of human platelets. *FEBS Lett.* 186: 175–179
46. Alzamora R, Marusic ET, Gonzalez M and Michea L (2003) Nongenomic effect of aldosterone on Na<sup>+</sup>,K<sup>+</sup>-adenosine triphosphatase in arterial vessels. *Endocrinology* 144: 1266–1272